Effects of Wettability on Three-Phase Flow in Porous Media†

Mun-Hong Hui‡

Department of Petroleum Engineering, Stanford University, Stanford, California 94305-2220

Martin J. Blunt*

Centre for Petroleum Studies, T. H. Huxley School, Imperial College, London, SW7 2BP U.K.

Received: September 17, 1999; In Final Form: December 1, 1999

We study the effects of rock wettability on the flow of oil, water, and gas in hydrocarbon reservoirs. We describe the three-phase fluid configurations and displacement processes in a pore of polygonal cross section. Initially water-filled, water-wet pores are invaded by oil, representing primary oil migration. Where oil directly contacts the solid surface, the surface will change its wettability. We then consider water injection followed by gas injection for any possible combination of oil/water, gas/water, and gas/oil contact angles. We find the capillary pressures for the different displacement processes and determine the circumstances under which the various fluid configurations are stable. Using empirical expressions for the phase conductances, we find three-phase relative permeabilites for a bundle of pores of different sizes with constant triangular cross sections. For gas injection, we show that the oil remains connected in wetting layers down to low oil saturation with a characteristic layer drainage regime, which gives very high ultimate oil recoveries. The only exceptions are nonspreading oils in water-wet media and large gas/oil contact angles. The relative permeability of the phase of intermediate wettability depends on two saturations, while the relative permeabilities of the other phases are functions of their own saturation only. In water-wet media, oil is the intermediate-wet phase. In weakly oil-wet media, water is intermediate-wet. In strongly oil-wet media, gas is intermediate-wet. This finding contradicts the assumptions made in many empirical models that gas is always the most nonwetting phase and that its relative permeability depends only on the gas saturation. This work indicates appropriate functional dependencies for three-phase relative permeabilities, and represents a necessary first step toward the development of a predictive pore-scale model that accounts for the effects of wettability in three-phase flow.

Introduction

The simultaneous flow of three phases—oil, water, and gas—occurs in a variety of circumstances during hydrocarbon extraction from underground reservoirs and contaminant migration in the unsaturated zone. Conventionally, hydrocarbon reservoirs are exploited through pressure decline (primary production) followed by water injection. If the pressure remains above the bubble point, then only oil and water are flowing. Typical oil recoveries for such processes are in the range of 20−50%,[1] which means that the oil is flowing at a relatively high saturation. In these cases, the oil relative permeability is of order 1 in most parts of the reservoir, and the overall recovery is controlled, to a first approximation, by the well placement and the geological structure. Improved oil-recovery schemes in which three-phase flow occurs, such as gas injection, gas cap expansion, and thermal flooding, attempt to boost the hydrocarbon recovery into the 50−80% range. In this case, the oil is flowing at much lower saturation, meaning that the oil relative permeability can be very low and may vary by orders of magnitude with small changes in saturation. For these situations, accurate predictions of the relative permeabilities are critical for making sound judgments of the project economics. The movement of non-aqueous-phase pollutants above the water table in a moist soil is another three-phase flow process that involves flow at low oil saturations.

Unfortunately, experimental measurements of three-phase properties are often difficult and time-consuming to obtain, particularly at low oil saturations.[1] Two independent fluid saturations are needed to define a three-phase system, leading to a large combination of different possible fluid arrangements. Moreover, the behavior is often critically dependent on the saturation path taken by the displacement (see, for instance, Oak et al.[2]). The standard practice in the oil industry is to use empirical models to predict three-phase relative permeability that are based on extrapolations from simpler two-phase measurements. As an example, in Prudhoe Bay, where significant oil recovery comes from three-phase gravity drainage and gas injection, experimental data on rock samples from the field in which all three phases are flowing simultaneously are quite sparse. However, extensive two-phase measurements have been made (for oil/water or gas/oil flow) that have been used to develop a detailed three-phase model.[3,4] The predicted three-phase relative permeabilities are then used in a numerical simulator to predict recovery in the field for different possible development strategies. Although this is a convenient approach for numerical simulation studies, predictions of the oil relative permeability from different three-phase models in the low saturation range of interest typically vary by orders of magnitude.[5,6] As a result, accurate assessment of improved oil recovery schemes is very difficult.

† Part of the special issue "Harvey Scher Festschrift".

* Corresponding author. Fax: 44 171 594 7444. E-mail: m.blunt@ic.ac.uk.
‡ Fax: 650 725 2099. E-mail: mun@pangea.stanford.edu.

10.1021/jp9933222 CCC: $19.00
Published on Web 02/17/2000

Physically based modeling of flow at the pore scale offers an appealing alternative to empirical models for predicting three-phase relative permeability. Micromodel experiments and theoretical analyses have elucidated the microscopic three-phase displacement mechanisms in uniformly water-wet and oil-wet media.[7−12] These studies have been the basis of pore network models that predict macroscopic parameters from the pore structure and the displacement physics.[13−17] This work assumed that the medium was strongly water-wet. In reality, oil reservoirs are rarely water-wet. One reason for this is that polar components of the crude oil adhere to rock surfaces and alter the rock wettability. This leads to variations in wettability at the pore scale and makes possible any gas/oil, oil/water, and gas/water contact angle.[18−20]

Two-phase (oil/water) pore network models for studying the effects of wettability have been developed by several authors. Any oil/water contact angle could be assigned to each pore in the network.[21−24] Kovscek et al.[25] developed a physically based model for wettability alteration at the pore scale. A primary drainage displacement was first simulated, assuming that the medium is initially fully water-saturated and water-wet. Where oil directly contacted the solid surface, the surface became strongly oil-wet. Regions of the pore where wetting layers or thick wetting films were present, as well as pores full of water, remained water-wet. Capillary pressures were computed for a bundle of star-shaped pores. Blunt extended this model to allow the regions of the pore space that were contacted by oil to assume any oil/water contact angle.[26,27] He computed relative permeabilites and capillary pressures for a three-dimensional network containing pores with a square cross section. Øren et al.[28] used a similar model of the displacement physics and wettability changes to simulate two-phase flow in a network with a random topology that was reconstructed from thin-section analysis. The predicted relative permeability of a mixed-wet reservoir rock agreed with experimental measurements. Man and Jing[29] studied the effects of wettability on electrical resistivity for networks of pores with a variety of shapes. Overall, the effects of wettability on relative permeability and oil recovery for two-phase flow are now reasonably well understood.[24,26]

This paper is one step in the three-phase extension of the two-phase work described above. The model of Kovscek et al.[25] and Blunt[26] will be used to find the pore-scale configurations of oil, water, and gas during waterflooding and gas injection, for the full range of possible oil/water, gas/oil, and gas/water contact angles. As in Kovscek et al.,[25] the general trends in behavior with wettability will be studied using a bundle-of-tubes model.

The purpose of this work is twofold. The description of fluid configurations, displacement capillary pressures, and conductances for three-phase mixed-wet pores is a necessary first step in the development of a predictive three-phase network model that will combine these displacement mechanisms with a realistic description of the pore space in a three-dimensional network. Second, the analysis of relative permeabilities, albeit from an idealized model, illustrates some general features that will be present in more sophisticated treatments. As such, they serve as a guide for the development of improved three-phase relative permeability predictions and as a means of interpreting experimental results.

First, the different possible pore-scale configurations will be described, and the capillary pressures for displacement from one configuration to another will be given. Then, the fluid saturations and conductances will be found. Finally, these results will be used in a bundle-of-capillary-tubes model to predict trends in three-phase relative permeability as the wettability of the system is modified.

Theoretical Approach

Representing the Pore Space. An exact representation of the complex geometry of the pore space for a mineralogically complex reservoir rock, combined with a model of possible crude oil/solid interactions, is a daunting task. However, it is possible to make progress by representing the void space of the rock as a lattice of interconnected pores. As a first step in network modeling, it is necessary to compute fluid configurations, displacement pressures, and phase conductances for pores of some simple shape. We will consider pores with a uniform polygonal cross section. Each corner of the polygon has a half-angle α. Later, we will consider one specific case: pores whose cross sections are equilateral triangles where $\alpha = 30°$. To place this approach in context, Øren and co-workers[28,30] have generated equivalent networks from images of the pore space taken from either microscopic X-ray tomography or numerical reconstruction. Although no pores are exactly polygonal in cross section, modeling them as having a triangular shape that has the same ratio of the square of the perimeter length to the cross-sectional area as the real pore is sufficient to enable accurate predictions of two-phase properties to be made. In this work, we will be interested in trends in relative permeability with wettability and will consider nothing more than a simplistic bundle-of-tubes model, so that a more accurate consideration of realistic pore geometries is not necessary. However, it is possible that extensions of this work, using the expressions for conductance and displacement pressures in this paper, could be used as the foundation of a predictive three-phase model if an irregular lattice of interconnected angular pores were considered.

The most important generic feature of angular pores, as opposed to those of circular cross section, is that the corner of the pores can be filled with wetting fluid, even if the centers are filled with another phase. As we will show later, flow through these wetting layers has a significant impact on relative permeability.

Wettability Changes. Most reservoirs are composed of rocks that are naturally water-wet. However, most reservoirs are either weakly water-wet or oil-wet.[31] A series of experimental studies on crude-oil/rock/brine systems and contact angle measurements for oil and water on a flat surface (see, for instance, refs 20 and 32) have suggested that the wettability of the reservoir rock changes as a result of the direct contact of crude oil with the solid surface. High-molecular-weight, polar compounds in the oil, called asphaltenes, can sorb to the solid, rendering the surface weakly water-wet or oil-wet. When oil is moving over the solid surface, the receding oil/water contact angle is close to zero. If, however, the system is then left to rest for several hours to days, the advancing oil/water contact angle, when water displaces oil, is much larger. The exact degree of wettabilty alteration depends on the mineralogy of the surface and the chemical composition of the oil. Heavy oils with a high asphaltene content (such as California crudes) give oil/water contact angles close to 180°, whereas lighter oils with a lower asphaltene content, such as North Sea oils, may give contact angles of less than 90°, meaning that the surface is water-wet.[20,32,33] In laboratory studies, the wettability change is complete after around 1000 h, which is much faster than the time scale for oil migration and production from the reservoir. Regions of the pore space that contain water, or regions where

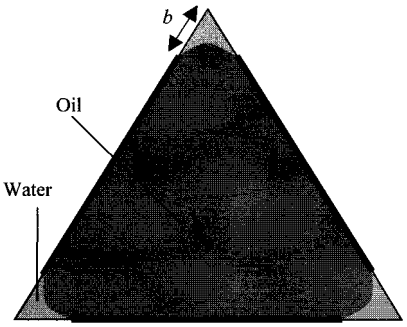

Figure 1. Oil and water in a triangular pore after primary drainage. The areas directly contacted by oil (shown by the bold line) have an altered wettability, whereas the corners that are water-filled remain water-wet. *b* is the length of the water-wet surface.

the surface is covered by a thick (several nanometers across) wetting film of water, remain water-wet.

The wettability change for a pore that contains oil is initiated by the collapse of a thick wetting film of water that covers the solid surfaces. This collapse occurs when the capillary pressure is sufficiently high to overcome the disjoining pressure of the film. We will model this process of wettability alteration in a single pore for a typical sequence of saturation changes in the reservoir, following the work of Kovscek et al.[25] and Blunt.[26] However, rather than consider disjoining pressure, which requires knowledge of molecular properties, we will simply assume that all surfaces in contact with oil will undergo a wettability change. We then allow any value to be assigned to the resultant advancing oil/water contact angle. If the surface is still coated by a thick wetting film, the oil/water contact angle will be close to zero.

Initially, all the pores are full of water, and the system is strongly water-wet. This condition represents the native state of the reservoir before primary oil migration. First, primary drainage, in which oil invades into the pore space, is simulated. Oil will displace water from a pore when the pressure difference between oil and water (the oil/water capillary pressure P_{cow}) reaches a critical value. The displacement capillary pressures for this process and for water flooding are given in the Appendix. Primary drainage continues with the water pressure increasing and the oil invading progressively smaller pores until some maximum oil/water capillary pressure P_{cow}^{max} is reached. The configuration of oil and water in a triangular pore at this stage is shown in Figure 1. It is assumed that, during primary drainage, surfaces of the pore that are in direct contact with oil alter their wettability. Small pores that are water-filled remain water-wet, as do the corners of the pores that still contain water. The oil/water contact angle for primary drainage is θ_1. It is assumed that $\theta_1 + \alpha < \pi/2$ and, thus, that water is always present in the corners. (Remember, this is the receding contact angle, where oil is moving over a water-coated surface.) Experimentally, θ_1 is always small.[20,32] The distance *b* of the water-wet surface in Figure 1 is given by

$$b = \frac{\sigma_{ow}}{P_{cow}^{max}}(\cot \alpha \cos \theta_1 - \sin \theta_1) \quad (1)$$

where σ_{ow} is the oil/water interfacial tension.

During waterflooding and gas injection, we will allow any value for the oil/water, gas/water, and gas/oil contact angles at the surfaces of altered wettability. While this is a simple model of wettability alteration, it captures one of the principal mechanisms for wettability alteration in reservoir settings,[18,20] and for two-phase flow, it has been shown to lead to macroscopic consequences that cover the full range of experimentally observed behavior.[24−27] The essential features of the model are that (1) different wettabilities can be present in a single pore, as shown by electron microscopy;[19] (2) any combination of contact angles can be considered; and (3) the mechanism of wettability alteration is the contact of crude oil with the solid surface.[18,20]

The different possible arrangements of the three phases in a single pore are illustrated in Figure 2. Configuration A represents a water-filled pore that was not invaded during primary drainage and, so, remains water-wet. We will assume that these pores are never invaded during gas injection, although such an invasion could be considered by setting the gas/water (water receding) contact angle $\theta_{gw} = 0$ in the equations that follow. Below, we will describe how the other configurations arise during water and gas injection. However, first, we will consider the possible values of contact angles for three-phase flow.

Possible Values of the Contact Angles. There is one constraint on the interfacial tensions and contact angles. Consider the oil/water/solid contact on a flat surface that is illustrated in Figure 3. A horizontal force balance gives the following relationship:

$$\sigma_{os} = \sigma_{ws} + \sigma_{ow} \cos \theta_{ow} \quad (2)$$

where σ_{ws} is the water/solid interfacial tension, σ_{os} is the oil/surface interfacial tension, and θ_{ow} is the oil/water contact angle. Contact angles are always measured through the denser phase (water for oil/water and gas/water systems and oil for gas/oil systems). We can consider equivalent situations with water/gas/solid and oil/gas/solid contacts to obtain

$$\sigma_{gs} = \sigma_{ws} + \sigma_{gw} \cos \theta_{gw} \quad (3)$$

$$\sigma_{gs} = \sigma_{os} + \sigma_{go} \cos \theta_{go} \quad (4)$$

where σ_{gs} is the gas/solid interfacial tension, σ_{go} is the gas/oil interfacial tension, and θ_{go} is the gas/oil contact angle. Adding eqs 2 and 4 and comparing with eq 3 leads to the following result:[34]

$$\sigma_{gw} \cos \theta_{gw} = \sigma_{go} \cos \theta_{go} + \sigma_{ow} \cos \theta_{ow} \quad (5)$$

Equation 5 assumes that all three phases are stationary and in thermodynamic equilibrium and that the interfacial tensions include the effects of any wetting and spreading films that may be present. It is not known how applicable this expression is when the contacts are moving over a rough and chemically heterogeneous surface. However, we will use it as a constraint on our values of contact angles when oil is receding and gas and water are advancing.

Contact Angles for a Water-Wet Medium. If the system is strongly water-wet, the solid surfaces are coated by a thick film of water, making $\sigma_{gs} = \sigma_{gw}$ and $\sigma_{os} = \sigma_{ow}$, which leads to the following expression for θ_{go} from eq 4:[35]

$$\cos \theta_{go} = \frac{\sigma_{gw} - \sigma_{ow}}{\sigma_{go}} = 1 + \frac{C_{so}}{\sigma_{go}} \quad (6)$$

where C_{so} is the oil spreading coefficient, defined by

$$C_{so} = \sigma_{gw} - \sigma_{ow} - \sigma_{go} \quad (7)$$

In thermodynamic equilibrium, where the gas/water interface may include a molecular spreading film of oil, $C_{so} \leq 0$.[36]

Contact Angles for an Oil-Wet Medium. Consider an oil-wet system in which the solid surfaces are coated by a thick oil

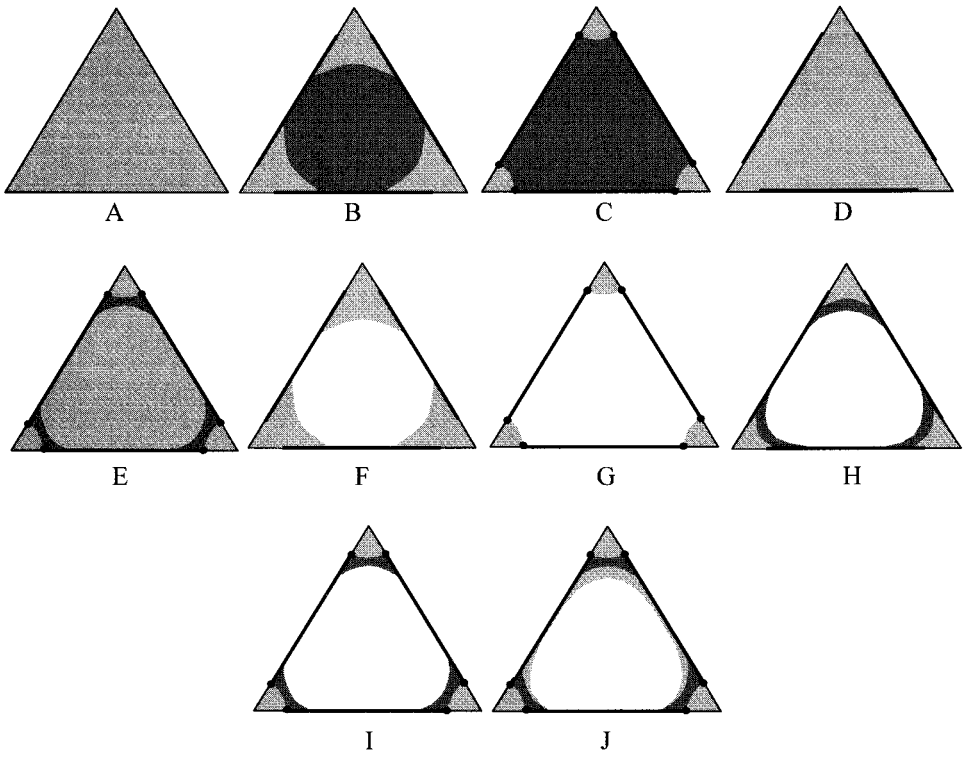

Figure 2. Different pore-scale configurations for water flooding and gas injection in mixed-wet pores. A bold line indicates regions of the pore space with altered wettability. The solid circles indicate points where the fluid/surface contact is pinned and the contact angle continually varies with capillary pressure. Light gray indicates water, dark gray indicates oil, and white indicates gas.

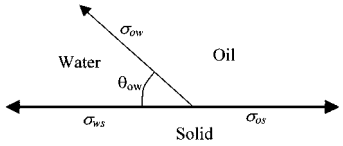

Figure 3. Three-phase oil/water/solid contact. A consideration of the horizontal balance of forces for this contact and the oil/gas/solid and water/gas/solid contacts leads to a relation between the interfacial tensions and contact angles, eq 5.

film. Then, in eq 5, $\sigma_{gs} = \sigma_{go}$ and $\sigma_{ws} = \sigma_{ow}$, which leads to the following result:

$$\cos \theta_{gw} = \frac{\sigma_{go} - \sigma_{ow}}{\sigma_{gw}} \tag{8}$$

For most fluid systems—particularly those at reservoir conditions for which σ_{go} may be very low for near miscible gas injection—$\sigma_{ow} > \sigma_{go}$, meaning that $\theta_{gw} > 90°$. Gas is wetting to water in strongly oil-wet media. Measurements of contact angles on oil-wet surfaces have found θ_{gw} in the range 100−120°, consistent with predictions based on eq 8.[37,38]

If we apply eq 5 with plausible values for the interfacial tensions, gas is only nonwetting to water for water-wet and weakly oil-wet media (θ_{ow} just above 90°).

Wettability Types. There are three different generic wettability types. The first is a water-wet system, for which gas is nonwetting to both water and oil ($\theta_{ow} < 90°$, $\theta_{go} < 90°$, and $\theta_{gw} < 90°$). In this case, water is the most wetting phase, gas is nonwetting, and oil is intermediate-wet. The second type is a strongly oil-wet medium, for which gas is wetting to water but nonwetting to oil ($\theta_{ow} > 90°$, $\theta_{go} < 90°$, and $\theta_{gw} > 90°$). In this case, oil is the most wetting phase, water is nonwetting, and gas is intermediate-wet. The third case is a weakly oil-wet medium, for which gas is nonwetting to both oil and water ($\theta_{ow} > 90°$, $\theta_{go} < 90°$, and $\theta_{gw} < 90°$). Oil is the wetting phase, gas is nonwetting, and water is intermediate-wet. On physical grounds, we do not consider cases in which gas is more wetting than oil. We will now explore the consequences of these different wettabilities on displacement pressures and relative permeability.

Water Flooding. The advancing oil/water contact angle for water flooding, θ_{ow}, may be larger than θ_1. As the oil/water capillary pressure decreases, the oil/water/solid contact is pinned with a hinging contact angle θ_h that increases from θ_1 to θ_{ow}. When $\theta_h = \theta_{ow}$, the oil/water/solid contact can move, and displacement may occur. There are three possible displacement mechanisms for pore filling: spontaneous snap-off, piston-like advance, and forced snap-off. The displacement processes are described, following the work of Blunt,[26] in the Appendix. Configurations A−E in Figure 2 show the possible arrangements of fluid. The Appendix describes the range of capillary pressures and contact angles for which the different patterns are seen. Configuration A is a pore that has always been full of water. In configurations B and C, the centers of the pore have not been invaded by water. However, the pores have experienced an increase in water saturation from the configuration in Figure 1. This is because the oil/water capillary pressure has decreased, leading to a swelling of the water layers and a change in the curvature of the oil/water interfaces. Configurations D and E are pores whose centers have been invaded by water. In configuration E, water occupies the center and corners of the pore, with layers of oil sandwiched in between.

Gas Injection. We assign gas/water and gas/oil contact angles, θ_{gw} and θ_{go}, respectively, for gas injection on the surfaces of altered wettability. During gas injection, the gas/water and gas/oil capillary pressures increase. We assume that $P_{cgw} = P_{cow} + P_{cgo}$, where P_{cgw} is the gas/water capillary pressure and P_{cgo} is the gas/oil capillary pressure. We also assume that the gas pressure is never high enough to displace water from water-

filled pores that have never had oil in them, represented by configuration A in Figure 2.

Gas Invasion into Water. If $\theta_{gw} < \pi/2 - \alpha$, gas may fill the center of a pore while water occupies the corners, without a pinned gas/water/solid contact. Gas invasion is a displacement from configuration D in Figure 2 to configuration F, or from configuration E to configuration J. The capillary pressure is obtained from the Mayer−Princen−Stowe theory[39−42] and comes from Ma et al.[43] (see the Appendix).

$$P_{cgw} = \frac{\sigma_{gw}}{R}\left[\cos\theta_{gw} + \sqrt{\frac{\tan\alpha}{2}(\sin 2\theta_{gw} - 2\theta_{gw} - 2\alpha + \pi)}\right] \quad (9)$$

For $\sigma_{gw} \geq \pi/2 - \alpha$, the gas/water/solid contact is pinned. Gas invasion is a displacement from configuration D in Figure 2 to configuration G, or from configuration E to configuration I. The capillary pressure is given by[43]

$$P_{cgw} = \frac{2\sigma_{gw}\cos\theta_{gw}}{R} \quad (10)$$

Gas Invasion into Oil. The displacement capillary pressures are similar to those for gas injection into water. If $\theta_{go} < \pi/2 - \alpha$, gas invasion is a displacement from configuration B to configuration H, or from configuration C to configuration I. There is a free gas/oil/solid contact, resulting in an oil layer sandwiched between water in the corners and gas in the center of the pore. The displacement capillary pressure is given by

$$P_{cgo} = \frac{\sigma_{go}}{R}\left[\cos\theta_{go} + \sqrt{\frac{\tan\alpha}{2}(\sin 2\theta_{go} - 2\theta_{go} - 2\alpha + \pi)}\right] \quad (11)$$

For $\theta_{go} \geq \pi/2 - \alpha$, oil layers cannot be formed. The displacement goes from configuration B to configuration F, or from configuration C to configuration G, at a capillary pressure given by

$$P_{cgo} = \frac{2\sigma_{go}\cos\theta_{go}}{R} \quad (12)$$

Layer Formation and Stability. For gas injection, there are three fluid configurations with layers of either oil or water, namely, H, I, and J in Figure 2. For oil layers to be present and sandwiched between water and gas, configurations H or I, we must have

$$\theta_{go} + \alpha < \frac{\pi}{2} \quad (13)$$

Configuration H in Figure 2 shows a layer of oil sandwiched between water and gas at a positive oil/water capillary pressure. Such a layer will only exist if

$$\theta_{ow} + \alpha < \frac{\pi}{2} \quad (14)$$

In configuration H, the oil/water contact has moved during water injection, so that it is no longer pinned. This is only true if the oil/water capillary pressure exceeds the value given by

$$P_{cow} = \frac{\sigma_{ow}(\cot\alpha\cos\theta_{ow} - \sin\theta_{ow})}{b} \quad (15)$$

Oil-layer stability depends on the ratio of oil/water to gas/oil interfacial curvatures.

$$R_o = \frac{r_{ow}}{r_{go}} = \frac{\sigma_{ow}P_{cgo}}{\sigma_{go}P_{cow}} \quad (16)$$

Oil layers are stable in configuration H for $R_o \leq R_{co}$ until the oil/water/solid and gas/oil/solid contact points meet, and the system goes from configuration H to configuration F.[14,37]

$$R_{co} = \frac{\cos(\theta_{go} + \alpha)}{\cos(\theta_{ow} + \alpha)} \quad (17)$$

if $\theta_{go} \geq \theta_{ow}$. For $\theta_{go} < \theta_{ow}$, the oil/water and gas/oil interfaces first meet at their centers. Again, we have a transition from configuration H to configuration F at a critical curvature ratio given by

$$R_{co} = \frac{\cos\theta_{go} - \sin\alpha}{\cos\theta_{ow} - \sin\alpha} \quad (18)$$

If the oil/water/solid interface is pinned, as in configuration I in Figure 2, the oil/water capillary pressure is less than the critical value given in eq 15. To determine oil-layer stability, we first find the hinging contact angle from the equation

$$\theta_h = \cos^{-1}\left(\frac{P_{cow}b\sin\alpha}{\sigma_{ow}}\right) - \alpha \quad (19)$$

If $\theta_{go} \geq \theta_h$, we use eq 17 with θ_h substituted for θ_{ow} to determine whether oil layers are stable. If $\theta_h > \theta_{go}$, we use eq 18 with θ_h substituted for θ_{ow}.

The final case is configuration J in Figure 2, in which there are layers of both water and oil. Oil-layer collapse is a transition from configuration J to configuration F. The criterion for oil-layer stability is given by eq A11 in the Appendix. The water layers are sandwiched between oil and gas. The stability for water layers is determined in the same way as for oil layers. Water-layer collapse is a transition from configuration J to configuration I. We only see water layers if the following two conditions are met:

$$\theta_{gw} + \alpha < \frac{\pi}{2} \quad (20)$$

$$\theta_{ow} > \frac{\pi}{2} + \alpha \quad (21)$$

Then, by defining

$$R_w = \frac{r_{ow}}{r_{gw}} = \frac{\sigma_{ow}P_{cgw}}{\sigma_{gw}P_{cow}} \quad (22)$$

we see that water layers are stable for $R_w \leq R_{cw}$, where

$$R_{cw} = \frac{\cos(\theta_{gw} + \alpha)}{\cos(\theta_{ow} + \alpha)} \quad (23)$$

for $\theta_{gw} \geq \pi - \theta_{ow}$. For $\theta_{gw} < \pi - \theta_{ow}$,

$$R_{cw} = \frac{\cos\theta_{gw} - \sin\alpha}{\cos\theta_{ow} + \sin\alpha} \quad (24)$$

Fluid Saturation and Conductance. We will compute the three-phase relative permeabilities as a function of saturation

for a bundle of parallel pores. The saturation of each phase is the sum of the cross-sectional areas of each phase in each pore, divided by the total areas of all the pores. The relative permeability is the sum of the conductances in each pore, divided by the sum of conductances that would exist if only a single phase fills all the pores.

The total area of a pore of inscribed radius R is given by

$$A_t = n_c R^2 \cot \alpha \tag{25}$$

where n_c is the number of corners in each pore.

Each pore has a fixed length L and has a fixed pressure difference ΔP imposed across each phase. The conductance g is defined by

$$Q = \frac{g}{\mu}\frac{\Delta P}{L} \tag{26}$$

where Q is the volume of fluid flowing per unit time and μ is the viscosity.

For a pore totally full of a single fluid, we use the following approximation for g, based on Poiseuille's law for flow in a circular cylinder:[44]

$$g = \frac{\pi(\sqrt{A_t/\pi} + R)^4}{128} \tag{27}$$

For a phase that occupies the center of the pore space, we use the same expression, but with A_t substituted by the area of the phase.

The area occupied by fluid occupying the corners of a pore with an interfacial radius of curvature r is given by

$$A_c = n_c r^2[\cos\theta(\cot\alpha\cos\theta - \sin\theta) + \theta + \alpha - \pi/2] \tag{28}$$

where θ is the contact angle. Equation 28 is valid for all values of θ.

If a nonwetting phase occupies the center of the pore and a wetting phase occupies the corners with $\theta + \alpha < \pi/2$, the wetting-phase conductance can be found from an approximate expression due to Zhou et al.[45]

$$g = \frac{A_c^2(1-\sin\alpha)^2(\phi_2\cos\theta - \phi_1)\phi_3^2}{12n_c\sin^2\alpha(1-\phi_3)^2(\phi_2 + f\phi_1)^2} \tag{29}$$

where

$$\phi_1 = \frac{\pi}{2} - \alpha - \theta \tag{30}$$

$$\phi_2 = \cot\alpha\cos\theta - \sin\theta \tag{31}$$

$$\phi_3 = \left(\frac{\pi}{2} - \alpha\right)\tan\alpha \tag{32}$$

The quantity f is used to indicate the boundary condition at the fluid/fluid interface. A value of $f = 1$ represents a no-flow boundary, while a value of $f = 0$ is a free boundary. We will assume $f = 1$ for all oil/water interfaces and $f = 0$ for all gas/water and gas/oil interfaces. These assumptions are in agreement with the results of two- and three-phase flow experiments in single capillary tubes.[37,45]

Although eq 29 is an algebraically complex expression, it can easily be used in network modeling studies to compute the conductance of the wetting fluid. It gives predictions close to the results from computations of the Navier−Stokes equation in a corner.[45,46]

For $\theta + \alpha > \pi/2$, the fluid/fluid interface bulges out into the center of the pore, and eq 29 is no longer valid. To find an approximate expression for the conductance in this case, we write eq 29 in terms of the corner area and α when $\theta = 0$, as follows:

$$g = \frac{A_c^2\tan\alpha(1-\sin\alpha)^2\phi_3^2}{12n_c\sin^2\alpha(1-\phi_3)(1+f\phi_3)^2} \tag{33}$$

We use this expression when $\theta + \alpha > \pi/2$, using eq 28 with the appropriate **non-zero** value of θ to find A_c.

Zhou et al.[45] also derived an expression for the conductance of an oil layer sandwiched between water and gas, as in configuration H of Figure 2. In this case, it is assumed that $\theta_{go} = \theta < \pi/2 - \alpha$ and that $\theta_{ow} = 0$. The conductance is given by

$$g = \frac{A_c^2(1-\sin\alpha)^2[\phi_2\cos\theta - \phi_1 - \cot\alpha(1-\phi_3)R_o^2]^3\phi_3^2}{12n_c\sin^2\alpha(1-\phi_3)^2(\phi_2\cos\theta - \phi_1)^2[\phi_2 + f_1\phi_1 - \cot\alpha(1-f_2\phi_3)R_o]^2} \tag{34}$$

where f_1 is the boundary condition at the gas/oil interface and f_2 is the boundary condition at the oil/water interface. R_o is given by eq 16. The corner area is the area of both the oil layer **and** the water in the corners. The corner area is found from eq 28 with $\theta = \theta_{go}$ and $r = r_{go} = \sigma_{go}/P_{cgo}$.

For cases with a non-zero oil/water contact angle, or for interfaces that bulge into the centers of the pore space, we use a modified version of eq 34 to find the oil-layer conductance. First, we rewrite eq 34 assuming zero contact angles, as follows:

$$g = \frac{A_o^3(1-\sin\alpha)^2\tan\alpha\phi_3^2}{12n_cA_c\sin^2\alpha(1-\phi_3)\left[1 + f_1\phi_3 - (1-f_2\phi_3)\sqrt{\frac{A_w}{A_c}}\right]^2} \tag{35}$$

where A_w is the area of water in the corners, as computed from eq 28 with $\theta = \theta_{ow}$ and $r = r_{ow} = \sigma_{ow}/P_{cow}$. A_o is the area of oil in the corners and is computed from the relation $A_o = A_c - A_w$, where A_c is given by eq 28 with $\theta = \theta_{go}$ and $r = r_{go} = \sigma_{go}/P_{cgo}$. Equation 35 is then used to find the oil-layer conductance. With a suitable substitution of subscripts, the same approach can be used for oil layers sandwiched between water, or for water layers, as described below.

These equations will form the basis of the analysis to follow. The conductance equations are approximate; for first-principles predictive modeling, it may be appropriate to use expressions based on solutions of the Navier−Stokes equation for each pore.[28,46]

Primary Drainage. For a pore completely full of water, eq 25 is used to find the water area in each pore, and eq 27 is used to compute the water conductance. For a pore with oil in the center and water in the corners, the water area is found from eq 28 with $\theta = \theta_1$ and $r = r_{ow} = \sigma_{ow}/P_{cow}$, and the water conductance is found from eq 29 with $\theta = \theta_1$ and $f = 1$. The oil area A_o is $A_t - A_c$. The oil conductance is found from eq 27, but with A_o substituted for A_t.

Water Flooding. If oil or water occupies the center of a pore, eq 27 is used to find the conductance, with A_t substituted by the oil or water area in the center of the pore. The area of fluid

in the pore center is the total area of the pore minus the area of water in the corners and minus the area of oil layers, if present.

To find the water areas in the corners, the hinging contact angle is first calculated from eq 19. If $\theta_h < \theta_{ow}$, then the oil/water/solid interface is pinned, and eq 28 is used to find the water area with $\theta = \theta_h$ and $r = r_{ow} = \sigma_{ow}/P_{cow}$. If $\theta_h \geq \theta_{ow}$, then eq 28 is used with $\theta = \theta_{ow}$. For $\theta + \alpha < \pi/2$, eq 29 is used to find the water conductance with $f = 1$. If $\theta + \alpha > \pi/2$, then eq 33 is used, again with $f = 1$.

If oil layers are present, as in configuration E in Figure 2, we use eq 35 to find the oil-layer conductance. In this case, $f_1 = f_2 = 1$. A_c is the area of the oil layer plus the area of water in the corners and is found from eq 28 with $\theta = \pi - \theta_{ow}$ and $r = r_{ow} = \sigma_{ow}/P_{cow}$. A_w is the water area in the corners. Equation 19 is used to find the hinging contact angle of the pinned contact, and then A_w is found from eq 28 with $\theta = \theta_h$ and $r = r_{ow} = \sigma_{ow}/P_{cow}$. The oil-layer area A_o is $A_c - A_w$.

With oil layers present, the water conductance and the water area have two components, one from water in the corners and the other from water in the pore center. The total areas and the conductances are the sums of these two contributions.

Gas Injection. Gas always occupies the center of the pore space. Thus, eq 27 is used for the gas-phase conductance with the area of gas A_g substituted for A_t. A_g is the total area of the pore minus the area of water in the corners and minus the area of any water and oil layers.

For configuration F in Figure 2, for which $\theta_{gw} + \alpha < \pi/2$, the water area in the corners is found from eq 28 with $\theta = \theta_{gw}$ and $r = r_{gw} = \sigma_{gw}/P_{cgw}$. The water conductance is found from eq 29 with $f = 0$ and $\theta = \theta_{gw}$.

For configuration G in Figure 2, the gas/water/solid interface is pinned. First, the hinging contact angle is computed using eq 19 with P_{cgw}/σ_{gw} substituted for P_{cow}/σ_{ow}. Equation 28 is used to find the water area with $\theta = \theta_h$ and $r = r_{gw} = \sigma_{gw}/P_{cgw}$. For $\theta_h + \alpha < \pi/2$, eq 29 is used to find the water conductance with $f = 0$. If $\theta_h + \alpha \geq \pi/2$, then eq 33 is used, again with $f = 0$.

For configuration H in Figure 2, we have $\theta_{ow} + \alpha < \pi/2$ and $\theta_{go} + \alpha < \pi/2$. Equation 28 is used to find the water area A_w with $\theta = \theta_{ow}$ and $r = r_{ow} = \sigma_{ow}/P_{cow}$. Equation 29 with $f = 1$ is used to find the water conductance with $A_c = A_w$. The area of water and oil in the corners A_c is found from eq 28 with $\theta = \theta_{go}$ and $r = r_{go} = \sigma_{go}/P_{cgo}$. The oil area $A_o = A_c - A_w$. Then, eq 35 with $f_1 = 0$ and $f_2 = 1$ is used to find the oil-layer conductance.

In configuration I in Figure 2, the oil/water/solid contact is pinned, and $\theta_{go} + \alpha < \pi/2$. The hinging contact angle is computed using eq 19. Equation 28 is used to calculate A_w with $\theta = \theta_h$ and $r = r_{ow} = \sigma_{ow}/P_{cow}$. Equation 33 with $f = 1$ is used for the water conductance with $A_c = A_w$. A_c is found from eq 28 with $\theta = \theta_{go}$ and $r = r_{go} = \sigma_{go}/P_{cgo}$. The oil area $A_o = A_c - A_w$. The oil-layer conductance is then found from eq 35 with $f_1 = 0$ and $f_2 = 1$.

In configuration J in Figure 2, we have water both in the corners and in a layer, as well as oil in a layer. The oil/water/solid contact is pinned, and $\theta_{gw} + \alpha < \pi/2$. The hinging contact angle is computed using eq 19. Equation 28 is used to calculate A_{wc}, the area of water in the corners, with $\theta = \theta_h$ and $r = r_{ow} = \sigma_{ow}/P_{cow}$. Equation 34 with $A_c = A_{wc}$ and $f = 1$ is used for the water conductance. The oil-layer conductance is computed as for configuration E. The area of oil plus water $A_o + A_{wc}$ is found from eq 28 with $\theta = \pi - \theta_{ow}$ and $r = r_{ow} = \sigma_{ow}/P_{cow}$. Equation 35 is used to find the oil-layer conductance with $A_c = A_o + A_{wc}$, $A_w = A_{wc}$, and $f_1 = f_2 = 1$. If the area of the water layer is A_{wl}, then the area of all the water and the oil layer $A_o + A_{wc} + A_{wl}$ is found from eq 28 with $\theta = \theta_{gw}$ and $r = r_{gw} = \sigma_{gw}/P_{cgw}$. Equation 35 with $f_1 = 0$ and $f_2 = 1$ is used to find the water-layer conductance by substituting A_o with A_{wl}, A_w with $A_o + A_{wc}$, and $A_c = A_o + A_{wc} + A_{wl}$. The total water conductance is the sum of the conductances of the water in the corners and the water layer. The total water area $A_w = A_{wc} + A_{wl}$.

TABLE 1: Parameters Used for the Distribution of the Inscribed Pore Radius, *R*, Eq 36

parameter	meaning	value
R_{min}	minimum pore radius	1 μm
R_{max}	maximum pore radius	18.5 μm
δ	exponent	0.8
γ	exponent	1.6

Network Model. We consider displacement in a parallel bundle of horizontally aligned pores. Each pore has the same length and has an equilateral triangular cross section ($\alpha = \pi/6$), but the pores have different inscribed radii. We use a truncated Weibull distribution with 50 pores, similar to that used by Fenwick and Blunt.[14] The inscribed pore radii are found from the equation

$$R = (R_{max} - R_{min})\{-\delta \ln[x(1 - e^{-1/\delta}) + e^{-1/\delta}]\}^{1/\gamma} + R_{min} \quad (36)$$

where x is a random number between 0 and 1. The parameters used in the distribution are shown in Table 1.

We simulate primary drainage, water flooding, and gas injection and compute relative permeabilities and capillary pressures as a function of saturation. We assume that the capillary pressures alone control the displacement sequence, an assumption that is applicable for low flow rates. We fill one pore at a time. During primary drainage, P_{cow} increases, and at each step, oil occupies pores with the lowest value of P_{cow} for displacement. Primary drainage ends when P_{cow} reaches P_{cow}^{max}, at which point the water occupies only a small number of the smallest pores and the corners of the larger, oil-filled pores. The water saturation at the end of primary drainage is 2% for all of the cases presented. This value was chosen arbitrarily, although none of the trends in behavior are affected by this choice of water saturation. The important features are that some pores remain water-filled and that water remains in the corners of all of the pores. During water flooding, P_{cow} decreases, and at each step water invades the pore with the highest value of P_{cow} for displacement. Because we consider only a bundle of tubes, all of which are accessible for displacement, we need only consider piston-like advance. Snap-off will occur in multidimensional networks only when piston-like advance is topologically impossible.[26] Water flooding ceases at an oil saturation value of S_{oi}. During gas flooding, the gas pressure increases. We fill pores in sequence, with the pore that will be invaded at the lowest gas pressure filled next. This may involve gas displacing oil, controlled by $P_{cgo} = P_g - P_o = P_g - P_w - P_{cow}$, or gas displacing water, controlled by $P_{cgw} = P_g - P_w$. We assume that, during gas injection, P_w is fixed, and P_{cow} remains constant at its value at the end of water flooding. The simulations continue until there is no further displacement of oil by gas.

We compute the relative permeability and saturation of each phase after each pore is filled. We use the layer stability equations to check whether layers of oil and/or water are present.

We study two fluid systems: one based on air/water/hexane and the other based on air/water/dodecane. The interfacial tensions used are shown in Table 2. Simulations are performed

TABLE 2: Interfacial Tensions for the Two Fluid Systems Studied[a]

system	σ_{gw} (mN/m)	σ_{go} (mN/m)	σ_{ow} (mN/m)
hexane	67	19	48
dodecane	71	23	51

[a] Data from Firincioglu et al.[37]

TABLE 3: Contact Angles and Initial Oil Saturations, S_{oi}, at the Beginning of Gas Injection for the Different Simulations Run[a]

case	system	θ_{ow} (deg)	θ_{go} (deg)	θ_{gw} (deg)	S_{oi}
1	hexane	20	0	17	0.90
2	hexane	20	0	17	0.35
3	dodecane	20	30	17	0.90
4	hexane	70	0	58	0.90
5	dodecane	70	30	58	0.90
6	hexane	180	0	116	0.90
7	hexane	180	0	116	0.35
8	hexane	95	0	77	0.90
9	hexane	95	0	77	0.35

[a] In all cases, $\theta_1 = 20°$.

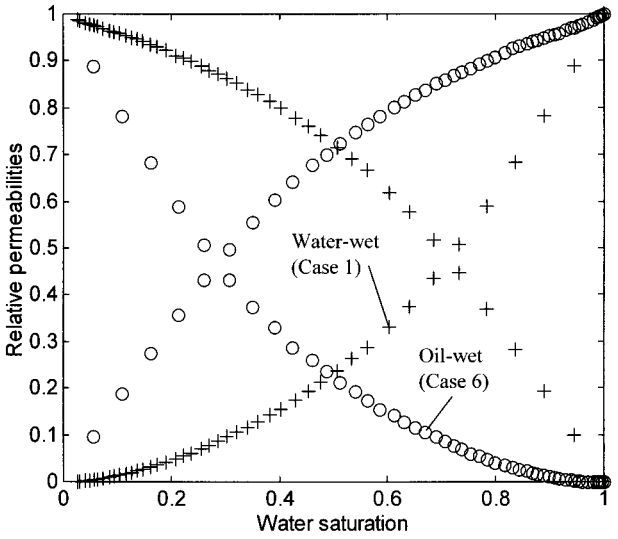

Figure 4. Two-phase relative permeabilities for water injection. The crosses are for a water-wet system, case 1 ($\theta_{ow} = 20°$), and the circles are for an oil-wet system, case 6 ($\theta_{ow} = 180°$).

for different combinations of contact angles and for different values of S_{oi}. The different properties used are listed in Table 3. We use eq 6 to assign θ_{go}, even if the system is not water-wet. We study the behavior for different values of θ_{ow}. Equation 5 is used to find θ_{gw}. This range of contact angles and interfacial tensions was used to cover the different types of generic behavior.

Results

Two-Phase Relative Permeability. Figure 4 shows the oil and water relative permeabilities for water injection for case 1 ($\theta_{ow} = 20°$) and case 6 ($\theta_{ow} = 180°$). For case 1, the water preferentially invades the smallest pores first. In contrast, for case 6, the water preferentially invades the largest pores, resulting in a higher water relative permeability and a lower oil relative permeability. The primary drainage relative permeabilities for all cases are the same as those for water injection for case 1.

A bundle-of-capillary-tubes model does not show any hysteresis, unless a wettability change occurs during the displacement sequence. Furthermore, no trapping of oil can be observed. Thus, the two-phase behavior of this model is rather simple. In particular, the nonwetting-phase relative permeability is overestimated. Using a three-dimensional network model would lower the predicted relative permeabilities to give curves that match experimental measurements,[26,27] but would not affect the trends in behavior that we describe for two- and three-phase flow. The same pore-level physics, used in a three-dimensional network, has shown complex hysteresis and a nonmonotonic trend in residual oil saturation with contact angle, which is consistent with experimental evidence.[26,27]

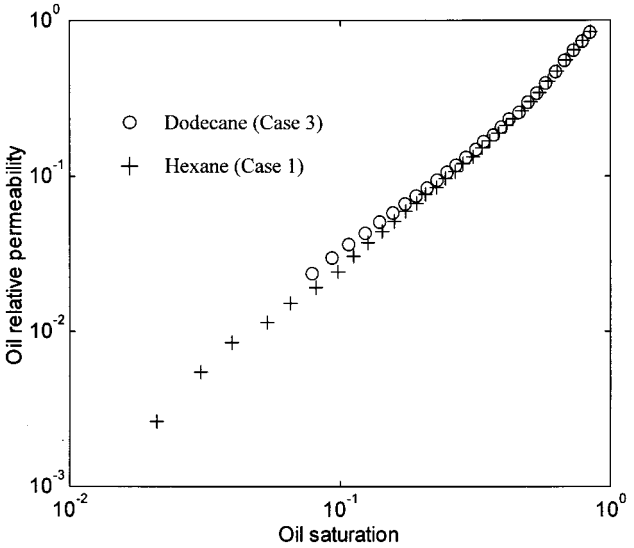

Figure 5. Oil relative permeability during gas injection in water-wet media. The curve for case 3 is stopped at an oil saturation value of $S_o = 0.08$, at which point oil layers collapse. For case 1, oil layers are present until a high gas/oil capillary pressure is reached, at which point the oil saturation is less than 1%.

Oil-Layer Drainage. Figure 5 shows the oil relative permeability during gas injection for water-wet media, cases 1 and 3. The difference between these two cases is the spreading coefficient of the oil, which manifests itself in different values of the gas/oil contact angle (Table 3). Oil layers collapse at a higher gas/oil capillary pressure for hexane ($R_{co} = 1.35$ in eq 18) than for dodecane ($R_{co} = 0.78$ in eq 17). This finding means that for hexane, oil layers remain until all of the oil-filled pores have been invaded by gas and very low oil saturations (less than 1%) are reached, whereas for dodecane, the oil saturation is around 8% when the layers collapse. In a three-dimensional network, the oil phase is likely to become disconnected when the layers are no longer present, and oil is likely to become trapped.[14,15]

Before the oil layers collapse, the dodecane relative permeability is slightly higher than that of hexane. For the same number of pores filled with gas, the hexane relative permeability is higher than that of dodecane, because the hexane oil layers make a greater contribution to the overall conductance. However, there is also more oil in these layers. If we compare relative permeabilities at the same oil saturation, this second effect dominates: hexane occupies fewer pores than dodecane, with the extra saturation coming from the layers. The extra conductance from these layers fails to compensate for the effect of having fewer oil-filled pores, making the hexane relative permeability slightly lower than that of dodecane. This counterintuitive effect, in which the possibility of layer flow decreases the oil relative permeability at moderate to low saturations, is apparent in three-phase core data.[6]

At low oil saturation, for case 1, we see that $k_{ro} \sim S_o^2$. This quadratic form of the relative permeability is a consequence of

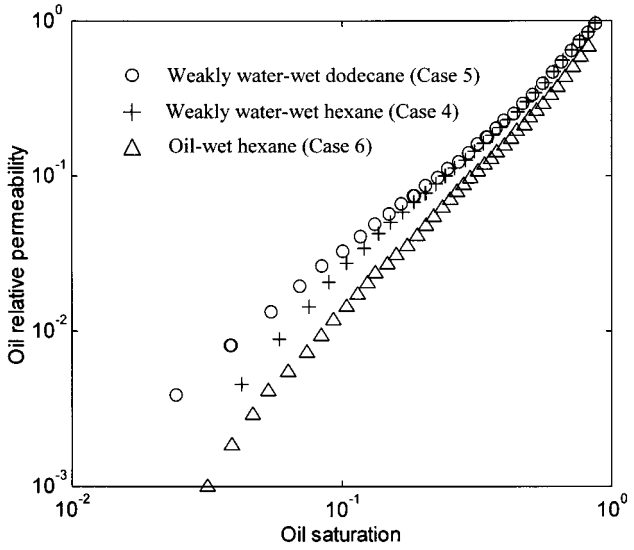

Figure 6. Oil relative permeability during gas injection showing the effect of oil/water contact angle. All three cases show a layer drainage regime to low oil saturation.

the expression used for oil-layer conductance, eq 35. Once gas has invaded most of the oil-filled pores, the oil saturation is approximately proportional to the oil area A_o. The oil-layer conductance (eq 35), and hence the relative permeability, is approximately, although not exactly, proportional to A_o^2, assuming that A_w is smaller than or roughly the same size as A_o. The effect of the spreading coefficient on oil recovery in water-wet media, as well as the quadratic behavior of the oil relative permeability, has already received extensive theoretical discussion[11,15,45] and has been confirmed experimentally.[11,37,38,47]

Figure 6 shows the oil relative permeability for intermediate-wet and oil-wet media, cases 4−6. We see oil-layer drainage to low saturation with an approximately quadratic form for the relative permeability for all of these cases, including the dodecane system. The oil/water/solid contacts are pinned, meaning that the oil/water interface cannot move to meet the gas/oil interface, which initiates layer collapse. Oil-layer collapse only occurs at a high gas/oil capillary pressure after gas has invaded all of the oil-filled pores and has pushed almost all of the oil out of the corners. An approximately quadratic oil relative permeability, consistent with the predictions described here, has been observed in mixed-wet sandpacks.[38] In these experiments, an initially water-wet and water-filled pack was invaded by a heavy crude oil. After aging, the crude was rinsed out, and three-phase gravity drainage using an octane/brine/air system was performed. The pattern of wettability at the pore scale is presumed to be similar to the model used here.

The oil relative permeability is sensitive to both the gas/oil and the oil/water contact angles. This fact is due to the equations used for oil-layer conductance and area. As before, the dodecane system has a slightly higher relative permeability, for the same reason as in Figure 5. The oil-wet hexane system has the lowest oil relative permeability. This is because the oil/water capillary pressure is negative, and so, the oil/water interface bulges out toward the gas/oil interface (configuration I of Figure 2). This leads to a lower oil-layer conductance compared with that of weakly water-wet systems, in which the oil/water interface bulges toward the corner because $P_{cow} > 0$. Notice the subtle competition between oil-layer area and conductance: in some cases, a large layer area tends to decrease relative permeability when comparing configurations with the same overall oil saturation, whereas in other cases, the greater conductance of these layers increases the relative permeability.

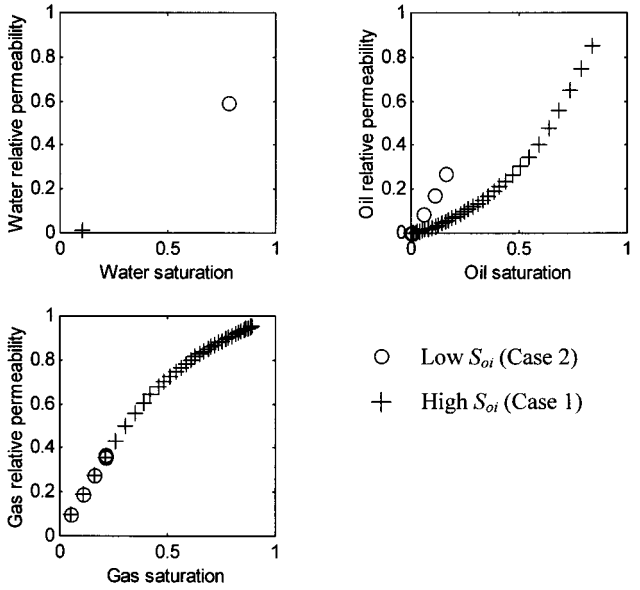

Figure 7. Three-phase relative permeabilities for a water-wet system. Oil is the intermediate-wet phase. The gas and water relative permeabilities do not depend on S_{oi}, whereas the oil relative permeability does. This result can be explained by considering the sizes of the pores occupied by each phase. See Figure 8.

The oil remains connected in layers during gas injection with a characteristic layer drainage regime. For three-dimensional systems, this will allow oil to drain to very low saturations, giving potentially high oil recoveries for gas injection. The two exceptions to this are nonspreading oils in water-wet media (case 3), or situations in which oil layers can never form, which we have not studied, so that eq 13 is not obeyed; instead, $\theta_{go} + \alpha > \pi/2$.

The full consequences of oil-layer connectivity and stability can only be explored using a three-dimensional network. The gas pressure at which layers collapse depends on the capillary pressure reached during primary drainage, through its effect on b, and the oil/water capillary pressure during water flooding. Hence, the oil relative permeability during gas injection may be sensitive to the entire previous displacement sequence.

Three-Phase Relative Permeabilities. While the relative permeability at low saturation may be dominated by layer drainage, the high-saturation behavior is controlled by the size of pores occupied by each phase. In the results that follow, we will see only three generic types of relative permeability. The first is for the wetting phase that occupies the smallest pores. The second is for the most nonwetting phase that occupies the largest pores. In both of these cases, the relative permeability is insensitive to S_{oi}. The relative permeability of the intermediate-wet phase lies between the wetting and nonwetting extremes and is function of both its own saturation and S_{oi}.

Oil Intermediate-Wet. Figure 7 shows the water, oil, and gas relative permeabilities for cases 1 and 2. Water is the wetting phase, gas is nonwetting, and oil is intermediate-wet. The gas relative permeability is a function of the gas saturation only and does not depend on S_{oi}. For water, because gas preferentially invades oil before water, we see only isolated values of the relative permeability. However, the points lie on the two-phase curve for a water-wet system (see Figure 4). The water relative permeability depends only on the water saturation.

To understand the oil relative permeability, consider the schematic pore occupancies shown in Figure 8. If S_{oi} is large, oil occupies almost all of the pores at the beginning of gas injection. Gas then invades the large oil-filled pores. Hence,

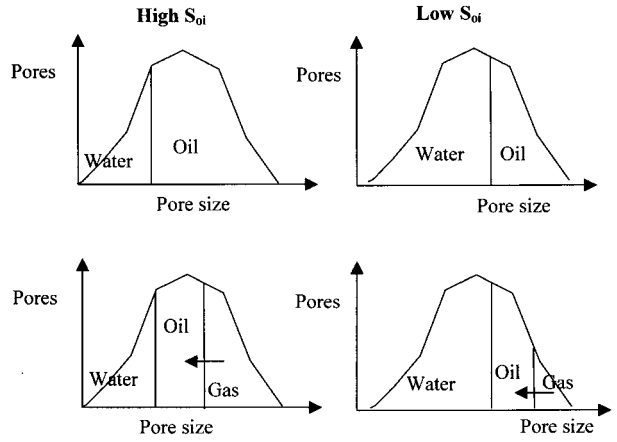

Figure 8. Schematic pore occupancies for a water-wet system. For two-phase flow, water resides in the small pores and oil in the large pores. During gas injection, the gas displaces oil from the largest pores. As the diagram shows, for the same oil saturation, oil will be in larger pores for low S_{oi} than for high S_{oi}, resulting in a higher oil relative permeability.

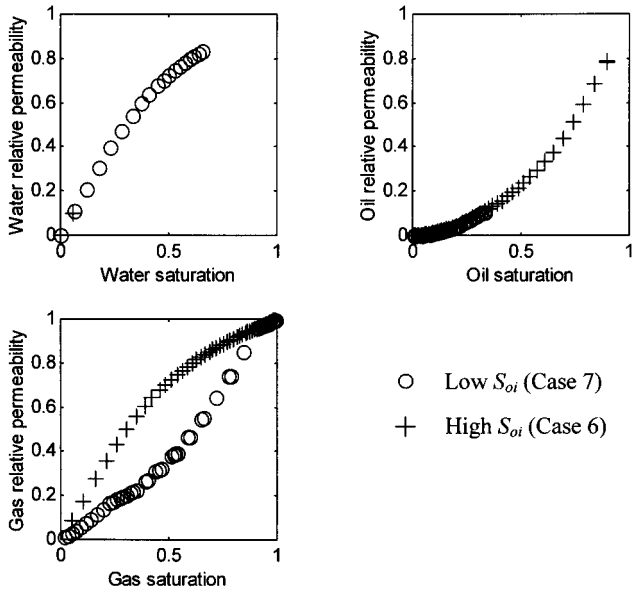

Figure 9. Three-phase relative permeabilities for a strongly oil-wet system. Gas is the intermediate-wet phase. The oil and water relative permeabilities do not depend on S_{oi}, whereas the gas relative permeability does.

oil is left filling the smaller pores. In contrast, if S_{oi} is small, oil occupies only the larger pores initially. While gas will preferentially invade the largest of these, at the same oil saturation, oil will occupy larger pores than those it occupies for a case with high S_{oi}, resulting in a higher oil relative permeability. The oil relative permeability for gas injection is, thus, a function of both S_o and S_{oi}, as shown in Figure 7. For modeling gas injection processes, this means that k_{ro} is a function of two independent saturations, whereas k_{rg} and k_{rw} are functions of their own saturations only. This observation is already well-known theoretically[2,5,6] and has been confirmed experimentally.[2,48−52]

Gas Intermediate-Wet. Figure 9 shows the three-phase relative permeabilities for cases 6 and 7, in which the system is strongly oil-wet. In these cases, oil is the most wetting phase, water is nonwetting, and gas is intermediate-wet. Using arguments similar to those used before, we see from Figure 9 that the oil relative permeability is similar to the water relative permeability for a water-wet system and is independent of S_{oi}.

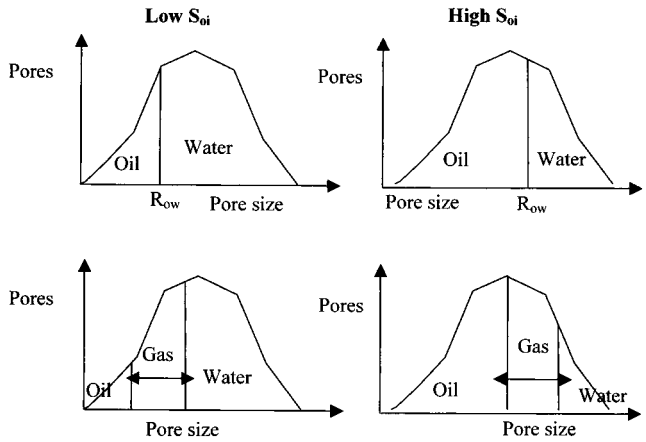

Figure 10. Schematic pore occupancies for an oil-wet system. For two-phase flow, oil resides in the small pores and water in the large pores. Gas is intermediate-wet. During gas injection, gas displaces both oil and water, starting by displacing pores with radii close to R_{ow}, the radius of the largest water-filled pore after water injection. For large S_{oi} and R_{ow}, gas occupies larger pores than for small S_{oi}, resulting in a larger gas relative permeability.

This result has been seen experimentally.[36] The water relative permeability is also independent of S_{oi} and is similar to the gas relative permeability in Figure 7, although the values are not identical because water continues to reside in the corners of the pores. Because gas is intermediate-wet, it is now the gas relative permeability that depends on both S_g and S_{oi}. This is an important observation, because many empirical models of three-phase relative permeability assume that the gas relative permeability is a function of gas saturation only.[3−5,53]

At the beginning of gas injection, we can compare the gas pressure necessary to enter a water-filled pore to that needed to enter an oil-filled pore. For gas to displace water, we use eq 10, as follows:

$$P_g = P_w + P_{cgw} = P_w + \frac{2\sigma_{gw}\cos\theta_{gw}}{R_{gw}} \qquad (37)$$

where R_{gw} is the inscribed radius of the pore to be filled by gas. For a gas/oil displacement,

$$P_g = P_w + P_{cow} + P_{cgo} \approx P_w + \frac{2\sigma_{ow}\cos\theta_{ow}}{R_{ow}} + \frac{2\sigma_{go}\cos\theta_{go}}{R_{go}} \qquad (38)$$

where R_{ow} is the inscribed radius of the pore last filled by water and R_{go} is the inscribed radius of the pore to be filled by gas. We have used approximate forms for the oil/water and gas/oil capillary pressures. Because the medium is oil-wet, R_{ow} will represent the smallest water-filled pore. Gas is wetting to water and so will want to fill this smallest pore. Hence, $R_{gw} = R_{ow}$. Gas is nonwetting to oil and so fills the largest oil-filled pores first. Hence, $R_{go} \approx R_{ow}$. We now compare eqs 37 and 38 with eq 5, to see that the gas pressures for displacing oil and water are about the same. This means that gas will displace both water and oil, starting with pores with a radius R_{ow}, which is determined by the capillary pressure at the end of water injection. This is shown schematically in Figure 10. If R_{ow} is large (large S_{oi}), then the gas relative permeability is higher than if R_{ow} is small (small S_{oi}), as seen in Figure 9. Notice that, for low S_{oi}, the points tend to come in bunches in Figure 9, with closely spaced points followed by larger gaps. A point is plotted each time a pore is filled. Gas is displacing both oil from small

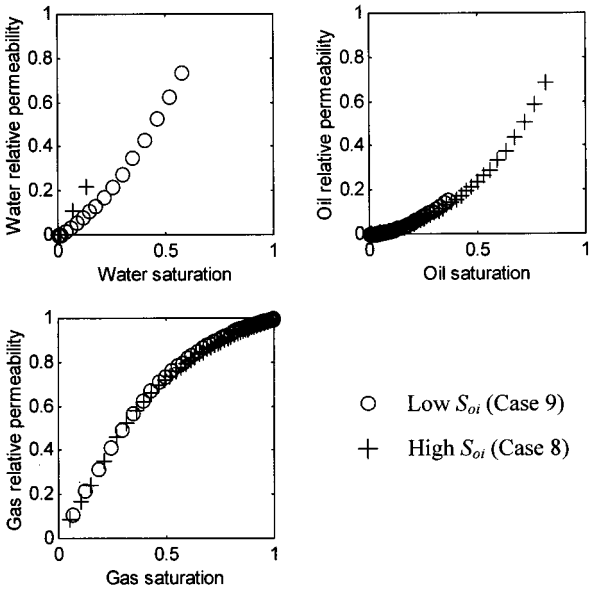

Figure 11. Three-phase relative permeabilities for a weakly oil-wet system. The gas and oil relative permeabilities do not depend on S_{oi}, whereas the water relative permeability does.

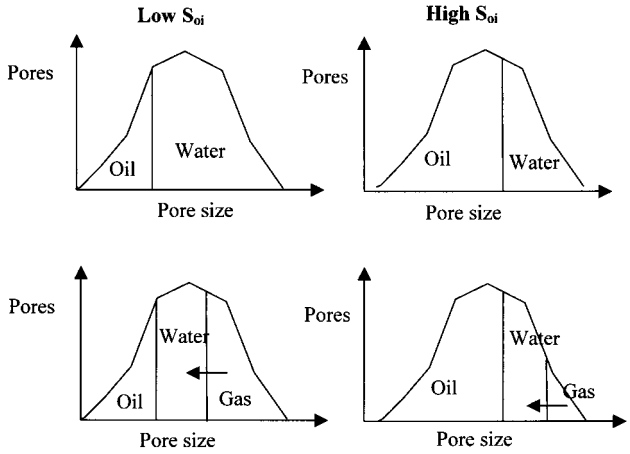

Figure 12. Schematic pore occupancies for a weakly oil-wet system. For two-phase flow, oil resides in the small pores and water in the large pores. Gas is nonwetting to oil and water. Gas invades the largest water-filled pores first. Water is intermediate-wet. For large S_{oi} water occupies larger pores than for small S_{oi}, at the same water saturation, resulting in a larger water relative permeability.

pores and water from large pores. The points close together represent the filling of the small pores, while the gaps represent the filling of the large pores.

Water Intermediate-Wet. Figure 11 shows the third generic combination of contact angles: an oil-wet system, in which gas is nonwetting to both water and oil. Gas always fills the largest pores, while oil resides in the smallest pores. Water is intermediate-wet, and its relative permeability is sensitive to S_{oi}, whereas the gas and oil relative permeabilities are functions of only their own saturations. The schematic pore occupancy is shown in Figure 12 and illustrates why the water relative permeability is higher for large S_{oi}, because, at the same water saturation, the water is in larger pores.

Fractionally Wet Media. Many porous media are fractionally wet, meaning that different regions of the pore space have different wettabilities. We could model this by allowing different pores to have different contact angles. For simplicity, we did not consider these cases. However, it is possible that with combinations of pores that fall into all three of the generic wettability types, the relative permeabilites of all three phases could be functions of two independent saturations. This observation has been confirmed from network modeling studies using pores of uniform wettability.[54] Empirical models of three-phase relative permeability must be able to allow all three relative permeabilities to depend on two saturations.[6,55]

Conclusions

We have found 10 fluid configurations in a single pore for three-phase flow in mixed-wet systems. The displacement sequence was primary drainage with wettability alteration followed by water flooding and gas injection. We found the capillary pressures for all possible displacements and analyzed oil- and water-layer formation and stability. We gave approximate expressions for the fluid conductances. This analysis is a first step in the development of a predictive pore-scale model of three-phase flow in mixed-wet media.

To illustrate the effects of wettability in three-phase flow, we computed relative permeabilites for a bundle of capillary tubes. The results for water-wet media, the quadratic oil-layer drainage regime and the effect of spreading coefficient, agree with previous theoretical and experimental work.[15,38,47]

Oil forms wetting layers in gas-occupied pores that persist down to low oil saturation with a characteristic layer drainage regime for the oil relative permeability. This observation has recently been confirmed for mixed-wet media.[38] The only exceptions are for nonspreading oils in water-wet media or for large gas/oil contact angles.

The relative permeability of the phase of intermediate wettability depends on both its own saturation and S_{oi}, whereas the relative permeabilities of the other phases are functions of their own saturation only. In water-wet media, oil is intermediate-wet. In weakly oil-wet media, water is intermediate-wet. In the most strongly oil-wet media, gas is intermediate-wet. For media that contain regions of different wettabilities, all three relative permeabilities may depend on both their own saturation and S_{oi}.

Acknowledgment. The authors are grateful to Pål-Eric Øren, Ken Sorbie, and Rink van Dijke for many helpful suggestions and comments. The members of the Stanford University Gas Injection Affiliates Group (SUPRI-C) and the Heriot-Watt/Stanford/Imperial consortium on pore-scale modeling (BP Amoco, Arco, Statoil, Elf, Enterprise Oil, Exxon, Shell, JNOC, and the Department of Trade and Industry) are thanked for their financial support.

Appendix: Two-Phase Displacement Processes

These mechanisms have already been described for mixed-wet pores by Blunt.[26] Here, we will use more accurate expressions for the capillary pressures for piston-like advance based on Øren et al.[28]

Primary Drainage. A pore of inscribed radius R fills with oil during primary drainage at a capillary pressure given by

$$P_{cow} = \frac{\sigma_{ow}}{R}\left[\cos\theta_1 + \sqrt{\frac{\tan\alpha}{2}}(\sin 2\theta_1 - 2\theta_1 - 2\alpha + \pi)\right] \quad \text{(A1)}$$

Spontaneous Snap-Off. During water flooding, spontaneous snap-off only occurs when $\theta_{ow} + \alpha < \pi/2$, which means that the water layer in the corner can swell at a positive oil/water capillary pressure (see configuration B in Figure 2). When the water layers lose contact with the solid surface, the pore

spontaneously fills with water to give configuration D. This occurs at an oil/water capillary pressure given by

$$P_{cow} = \frac{\sigma_{ow}(\cos\theta_{ow} - \sin\theta_{ow}\tan\alpha)}{R} \quad \text{(A2)}$$

Forced Snap-Off. Forced snap-off occurs for $P_{cow} < 0$, when $\theta_{ow} + \alpha \geq \pi/2$. Here the oil/water/solid contact point remains pinned (see configuration C in Figure 2), and the hinging contact angle varies continually with capillary pressure until the oil/water contact angle reaches θ_{ow}, at which point the oil/water interface bulges out into the center of the pore. When the hinging contact angle is θ_{ow}, the oil/water/solid contact begins to move, and the pore spontaneously fills with water to reach configuration D. The capillary pressure for this displacement is given by

$$P_{cow} = \frac{\sigma_{ow}(\cot\alpha\cos\theta_{ow} - \sin\theta_{ow})}{b} \text{ for } \pi - \alpha \geq \theta_{ow} \geq \pi/2 - \alpha$$

$$= -\frac{\sigma_{ow}}{b\sin\alpha} \text{ for } \theta_{ow} > \pi - \alpha \quad \text{(A3)}$$

Piston-Like Advance. The displacement capillary pressures for piston-like advance during water flooding are found from the Mayer−Stowe−Princen (MSP) theory.[39−42] There are three different expressions for these pressures, depending on the contact angle. For contact angles less than a critical value θ_{crit}, water spontaneously imbibes into the pore with a positive capillary pressure. After invasion, the pore is completely filled with water; the displacement goes from configuration B or C to configuration D in Figure 2. The value of θ_{crit} may be greater than $\pi/2$, as water advances into pores containing both water in the corners, where the effective contact angle is zero, and bare surfaces along the sides, where the contact angle is θ_{ow}. The critical angle for spontaneous imbibition, θ_{crit}, is given by

$$\cos\theta_{crit} = -\frac{\sin(\alpha + \theta_1)\sin\alpha}{\frac{RP_{cow}^{\max}}{\sigma_{ow}}\cos\alpha - \cos(\alpha + \theta_1)} \quad \text{(A4)}$$

To obtain the capillary pressure for the displacement, the following equations are solved:

$$P_{cow} = \frac{\sigma_{ow}\Omega_{eff}}{A_{eff}} = \frac{\sigma_{ow}}{r} \quad \text{(A5)}$$

where r is the effective mean radius of curvature,

$$A_{eff} = \frac{R^2}{2\tan\alpha} - \frac{rb\sin(\alpha + \beta)}{2} + \frac{r^2\beta}{2} \quad \text{(A6)}$$

$$\Omega_{eff} = \left(\frac{R}{\tan\alpha} - b\right)\cos\theta_{ow} + r\beta \quad \text{(A7)}$$

$$r\sin\beta = b\sin\alpha \quad \text{(A8)}$$

To solve these equations, P_{cow} is first computed assuming that $r = R$. Then, eqs A6 and A7 are used to find a new value of r from eq A5. Converged values of r and P_{cow} to three significant figures are normally found in just three iterations.

For $\theta_{ow} > \theta_{crit}$, water injection is forced, with a negative capillary pressure. For $\pi/2 + \alpha \geq \theta_{ow} > \theta_{crit}$, the displacement is from configuration C to configuration D in Figure 2, at a capillary pressure given by

$$P_{cow} = \frac{2\sigma_{ow}\cos\theta_{ow}}{R} \quad \text{(A9)}$$

Oil-Layer Formation and Stability. After piston-like advance with $\theta_{ow} > \pi/2 + \alpha$, there is water in the center of the pore and water in the corners, with a layer of oil sandwiched between them (see configuration E in Figure 2). The capillary pressure for displacement in this case is similar to eq A1 for primary drainage, as follows:

$$P_{cow} = \frac{\sigma_{ow}}{R}\left[\cos\theta_{ow} - \sqrt{\frac{\tan\alpha}{2}(-\sin 2\theta_{ow} + 2\theta_{ow} - 2\alpha - \pi)}\right] \quad \text{(A10)}$$

The oil layers are stable until the two arcs touch each other, when it is assumed that the layers spontaneously collapse. We go from configuration E to configuration D. This occurs at a capillary pressure given by

$$P_{cow} = \frac{\sigma_{ow}\left[\cos\alpha\sin\alpha(2\sin\alpha + \cos\theta_{ow}) + \sin^2\alpha \times \sqrt{4\cos^2\alpha - 3 - \cos^2\theta_{ow} - 4\sin\alpha\cos\theta_{ow}}\right]}{b(3\sin^2\alpha + 4\sin\alpha\cos\theta_{ow} + \cos^2\theta_{ow})} \quad \text{(A11)}$$

References and Notes

(1) Dullien, F. A. L. *Porous Media: Fluid Transport and Pore Structure*, 2nd ed.; Academic Press: San Diego, 1992.

(2) Oak, M. J.; Baker, L. E.; Thomas, D. C. *J. Pet. Technol.* **1990**, *42*, 1057.

(3) Jerauld, G. R. General Three-Phase Relative Permeability Model for Prudhoe Bay. Proceedings of the 7th ADIPEC, Abu Dubai, United Arab Emirates, October 13−16, 1996; SPE 36178.

(4) Jerauld, G. R. *SPE Reservoir Eng.* **1997**, *12*, 66.

(5) Baker, L. E. Three-Phase Relative Permeability Correlations. Proceedings of the SPE/DOE Symposium on Enhanced Oil Recovery, Tulsa, OK, April 17−20, 1988; SPE 17369.

(6) Blunt, M. J. An Empirical Model for Three-Phase Relative Permeability. Proceedings of the SPE Annual Conference, Houston, TX, 1999; SPE 56474.

(7) Øren, P.-E.; Billiote, J.; Pinczewski, W. V. *SPE Form. Eval.* **1992**, *7*, 70.

(8) Øren, P.-E.; Pinczewski, W. V. *Transp. Porous Media* **1995**, *20*, 105.

(9) Soll, W. E.; Celia, M. A.; Wilson, J. L. *Water Resour. Res.* **1993**, *29*, 2963.

(10) Kantzas, A.; Chatzis, I.; Dullien, F. A. L. Enhanced Oil Recovery by Inert Gas Injection. Proceedings of the Sixth SPE/DOE Symposium on Enhanced Oil Recovery, Tulsa, OK, April 1988; SPE 13264.

(11) Dong, M.; Dullien, F. A. L.; Chatzis, I. *J. Colloid Interface Sci.* **1995**, *172*, 278.

(12) Keller, A. A.; Blunt, M. J.; Roberts, P. V. *Transp. Porous Media* **1997**, *20*, 105.

(13) Heiba, A. A.; Davis, H. T.; Scriven, L. E. Statistical Network Theory of Three-Phase Relative Permeabilities. Proceedings of the SPE/DOE Symposium on Enhanced Oil Recovery, Tulsa, OK, April 15−18, 1984; SPE 12690.

(14) Fenwick, D. H.; Blunt, M. J. *Adv. Water Resour.* **1998**, *25*, 121.

(15) Fenwick, D. H.; Blunt, M. J. *SPEJ* **1998**, *3*, 86.

(16) Mani, V.; Mohanty, K. K. *SPEJ* **1998**, *3*, 238.

(17) Øren, P.-E.; Billiote, J.; Pinczewski, W. V. Pore-Scale Network Modelling of Waterflood Residual Oil Recovery by Immiscible Gas Flooding. Proceedings of the Ninth SPE/DOE Symposium on Improved Oil Recovery, Tulsa, OK, April 1994; SPE/DOE 27814.

(18) Morrow, N. R.; Lim, H. T.; Ward, J. S. *SPE Form. Eval.* **1986**, *1*, 89.

(19) Fassi-Fihri, O.; Robin, M.; Rosenberg, E. Wettability Studies at the Pore Level: A New Approach by the Use of Cryo-Scanning Electron Microscopy. Proceedings of the SPE Annual Conference, Dallas, TX, 1991; SPE 22596.

(20) Buckley, J. S.; Liu, Y. *J. Pet. Sci. Eng.* **1998**, *20*, 155.

(21) Mohanty, K. K.; Salter, S. J. Multiphase Flow in Porous Media: Part 3 − Oil Mobilization, Transverse Dispersion and Wettability. Proceedings of the SPE Annual Conference, San Francisco, CA, 1983; SPE 12127.

(22) Heiba, A. A.; Davis, H. T.; Scriven, L. E. Effect of Wettability on Two-Phase Relative Permeabilities and Capillary Pressures. Proceedings of the SPE Annual Conference, San Francisco, CA, 1983; SPE 12172.
(23) McDougall, S. R.; Sorbie, K. S. *SPE Reservoir Eng.* **1995**, *10*, 208.
(24) Dixit, A. B.; McDougall, S. R.; Sorbie, K. S.; Buckley, J. S. *SPE Reservoir Eval. Eng.* **1999**, *2*, 25.
(25) Kovscek, A. R.; Wong, H.; Radke, C. J. *AIChE J.* **1993**, *39*, 1072.
(26) Blunt, M. J. *SPEJ* **1997**, *2*, 494.
(27) Blunt, M. J. *J. Pet. Sci. Eng.* **1998**, *20*, 117.
(28) Øren, P.-E.; Bakke, S.; Arntzen, O. J. *SPEJ* **1998**, *3*, 324.
(29) Man, H. N.; Jing, X. D. *J. Pet. Sci. Eng.* **2000**, *24*, 255.
(30) Bakke, S.; Øren, P.-E. *SPEJ* **1997**, *2*, 136.
(31) Anderson, W. G. *J. Pet. Technol.* **1986**, 1125.
(32) Buckley, J. S.; Bousseau, C.; Liu, Y. *SPEJ* **1996**, *1*, 341.
(33) Kaminsky, R.; Radke, C. J. *SPEJ* **1997**, *2*, 485.
(34) Zhou, D.; Blunt, M. J. *J. Contam. Hydrol.* **1997**, *25*, 1.
(35) Kalaydjian, F. J.-M.; Moulu, J.-C.; Vizika, O. Three-phase Flow in Water-Wet Porous Media: Determination of Gas/Oil Relative Permeabilities Under Various Spreading Conditions. Proceedings of the SPE Annual Meeting, Houston, TX, October 3−6, 1993; SPE 26671.
(36) Adamson, A. W. *Physical Chemistry of Surfaces*, 5th ed.; John Wiley & Sons: New York, 1990.
(37) Firincioglu, T.; Blunt, M. J.; Zhou, D. *Colloids Surf., A* **1999**, *155*, 259.
(38) DiCarlo, D. A.; Sahni, A.; Blunt, M. J. *SPEJ* **2000**, *5*, in press.
(39) Mayer, R. P.; Stowe, R. A. *J. Colloid Interface Sci.* **1993**, *20*, 893.
(40) Princen, H. M. *J. Colloid Interface Sci.* **1969**, *30*, 60.
(41) Princen, H. M. *J. Colloid Interface Sci.* **1969**, *30*, 359.
(42) Princen, H. M. *J. Colloid Interface Sci.* **1970**, *34*, 171.
(43) Ma, S.; Mason, G.; Morrow, N. R. *Colloids Surf., A* **1996**, *117*, 273.
(44) Bryant, S.; Blunt, M. J. *Phys. Rev. A* **1992**, *46*, 2004.
(45) Zhou, D.; Blunt, M.; Orr, F. M., Jr. *J. Colloid Interface Sci.* **1997**, *187*, 11.
(46) Ransohoff, T. C.; Radke, C. J. *J. Colloid Interface Sci.* **1988**, *121*, 392.
(47) Sahni, A.; Burger, J. E.; Blunt, M. J. Measurement of Three-phase Relative Permeability during Gravity Drainage Using CT Scanning. Proceedings of the SPE/DOE 11th Symposium on Improved Oil Recovery, Tulsa, OK, April 1998; SPE 39655.
(48) Oak, M. J. Three-Phase Relative Permeability of Water-Wet Berea Sandstone. Proceedings of the SPE/DOE Seventh Symposium on Enhanced Oil Recovery, Tulsa, OK, April 22−25, 1990; SPE 20183.
(49) Baker, L. E. Three-Phase Relative Permeability of Water-Wet, Intermediate-Wet and Oil-Wet Sandstone. Proceedings of the 7th European Symposium on Improved Oil Recovery, Moscow, October 1993.
(50) Skauge, A.; Eleri, O. O.; Graue, A.; Monstad, P. Influence of Connate Water on Oil Recovery by Gravity Drainage. Proceedings of the SPE/DOE Ninth Symposium on Improved Oil Recovery, Tulsa, OK, April 17−20, 1994; SPE 27817.
(51) Eleri, O. O.; Graue, A.; Skauge, A. Steady-State and Unsteady-State Two-Phase Relative Permeability Hysteresis and Measurements of Three-Phase Relative Permeabilities Using Imaging Techniques. Proceedings of the SPE Annual Meeting, Dallas, TX, October 22−25, 1995; SPE 30764.
(52) Nordtvedt, J. E.; Ebeltoft, E.; Iversen, J. E.; Sylte, A.; Urkedal, H.; Vatne, R. F. Determination of Three-Phase Relative Permeabilities From Displacement Experiments. Proceedings of the Annual Technical Conference and Exhibition of the Society of Petroleum Engineers, Denver, CO, October 6−9, 1996; SPE 36683.
(53) Stone, H. L. *J. Pet. Technol.* **1970**, 214.
(54) van Dijke, R.; McDougall, S.; Sorbie, K. S. A Process-Based Approach for Three-Phase Capillary Pressure and Relative Permeability Relationships in Mixed-Wet Systems. Proceedings of the SPE/DOE Symposium on Improved Oil Recovery, Tulsa, April 2000; SPE 58030.
(55) Hustad, O. S.; Hansen, A. G. A Consistent Correlation for Three-phase Relative Permeabilities and Phase Pressures Based on Three Sets of Two-Phase Data. Proceedings of the Eighth European Symposium on Improved Oil Recovery, Vienna, Austria, May 15−17, 1995.